Inorganic Chemistry

Article

pubs.acs.org/IC

Stereodynamics in Eight-Coordination; A 2D NMR Spectroscopic and Computational Study of the Exchange Process in $ThCl_4(Me_2NCH_2CH_2NMe_2)_2$

Graham E. Ball*,[†] and Richard A. Andersen*,[‡]

[†]School of Chemistry, University of New South Wales (UNSW), Sydney, New South Wales 2052, Australia

[‡]Department of Chemistry and Chemical Sciences Division of Lawrence Berkeley National Laboratory, University of California, Berkeley, California 94720-1460, United States

Supporting Information

ABSTRACT: The $^{13}C\{^1H\}$ NMR spectrum of eight-coordinate $ThCl_4(tmed)_2$, where tmed = $Me_2NCH_2CH_2NMe_2$, shows that two isomers are present at 219.8 K in a ratio of ≈8:1 and inversion of the five-membered Th-tmed ring is slow at this temperature in both isomers. The 2D $^{13}C\{^1H\}$ exchange spectroscopy (EXSY) spectrum shows that each of the two inequivalent methyl groups of the major isomer does not exchange directly with each other but that they both exchange with both of the two inequivalent methyl groups found in the minor isomer. This implies that interconversion of the two enantiomers of the major isomer proceeds by a stepwise process that involves the minor isomer. The interconversion of the isomers involves a ring-inversion process that may proceed with or without Th−N bond breaking, and the NMR spectra cannot distinguish between these two processes nor can density functional theory (DFT) calculations (B3PW91 and M06 with consideration of dispersion effects and solvent) because these two possibilities proceed by way of transition states of similar energies in this case.

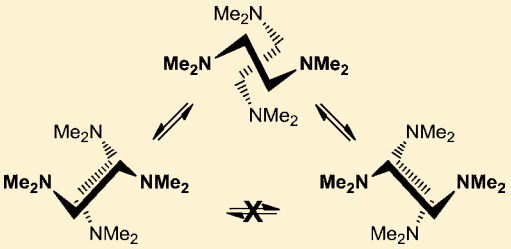

INTRODUCTION

The solid-state structures of eight-coordinate complexes have a range of geometries that have been reviewed,[1] and the deviations from idealized geometries are often determined by the shape parameters δ' and ϕ.[2,3] In solution, eight-coordinate complexes are usually stereochemically nonrigid or fluxional because the barriers for intramolecular rearrangements are inevitably small.[4,5] For example, uranium tetraacetylacetonate, $U(acac)_4$, exists in the solid state in two crystalline forms, α and β, in which the geometry of the UO_8 core resembles a bicapped trigonal prism and a square antiprism, respectively.[6−8] In solution, $U(acac)_4$ shows a single methyl resonance in the ^1H NMR spectrum that decoalesces into two resonances in the temperature range of 113−168 K, $\Delta G^{\ddagger}_{163\ K}$ = 7.2 kcal mol^{-1}.[9] In contrast, the ^1H NMR spectrum of diamagnetic $Th(acac)_4$ is dynamic down to 103 K! The fluxionality in coordination complexes that contain bidentate ligands with five-membered chelate rings has been studied extensively by NMR methods.[10] In general, the inversion rates depend on the substituents on the ligating atoms in the chelating bidentate ligands; in particular, the inversion barrier in complexes with a *N,N,N′,N′*-tetramethylethylenediamine (tmed) ligand can be determined by 1D NMR methods. The inversion barriers in $M(CO)_4(tmed)$ (M = Cr, Mo, W), range from 8.9 to 9.3 kcal mol^{-1} ($\Delta G^{\ddagger}_{300\ K}$).[11] In the four-coordinate complexes $[Co(tmed)(NO)_2]^+$ and $[Zn(tmed)Cl_2]$, $\Delta H^{\ddagger}_{187\ K}$ = 8.8 kcal mol^{-1}.[12] Of particular relevance to the subject matter of this Article, the inversion barrier in the eight-coordinate complex $Pr(fod\text{-}d_9)_3(tmed)$, where fod-$d_9$ is 6,6,7,7,8,8,8-heptafluoro-2,2-dimethyloctane-3,5-dionate-d_9, is $\Delta G^{\ddagger}_{235\ K}$ = 10.1 kcal mol^{-1}.[13,14]

The 2:1 tmed/metal complexes of uranium and thorium, $MCl_4(tmed)_2$, are useful complexes for synthetic studies because they are soluble in aromatic and chlorinated hydrocarbon solvents;[15a] $ThCl_4(tmed)_4$ was used recently in the synthesis of thorium metallocene compounds.[15b,c] Solubility also leads to the possibility of extraction with these organic solvents. Given the serious and increasing interest in using thorium as a nuclear fuel,[16−18] all coordination chemistry associated with thorium (indeed actinides, in general) that may relate to its processing/recovery is of considerable interest and importance. The crystal structure of $UCl_4(tmed)_2$ shows that the geometry of the eight-coordinate complex is close to that of a dodecahedron, based upon the shape parameters, with the N atoms on the A sites and the Cl atoms on the B sites.[19] The thorium complex is likely to have a similar structure because the IR spectra of the two complexes are superimposable. Both complexes are fluxional in solution because the Me_2N resonances appear as singlets at 293 K but they decoalesce into more than one resonance at low temperature in the 1D ^1H NMR spectra recorded at 90 MHz.[15a]

These preliminary studies were augmented by a more detailed 2D NMR spectroscopic study of the diamagnetic

Received: March 20, 2012
Published: September 19, 2012

thorium complex at higher field, the results of which are reported in this Article, along with density functional theory (DFT) calculations of the mechanism of the ring-inversion process. This paper demonstrates that while "eight coordinate structures are usually fluxional",[20] examples can be found where such fluxional processes can be slowed and mechanistic information extracted.

RESULTS AND DISCUSSION

Exchange Process from NMR Spectroscopy (EXSY). The 400 MHz 1D ^{1}H NMR spectrum of $ThCl_4(tmed)_2$ (**1**) in CD_2Cl_2 at 219.8 K (measured temperature) is shown in Figure 1.

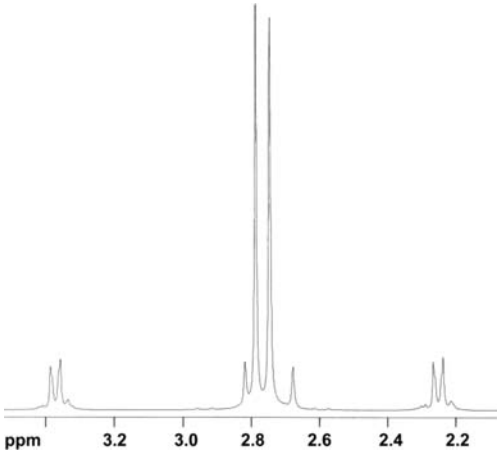

Figure 1. 400.1 MHz 1D ^{1}H NMR spectrum of **1** in CD_2Cl_2 at 219.8 K.

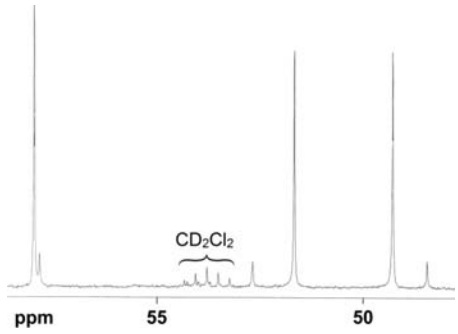

Figure 2. 100.6 MHz 1D $^{13}C\{^1H\}$ NMR spectrum of **1** in CD_2Cl_2 at 219.8 K.

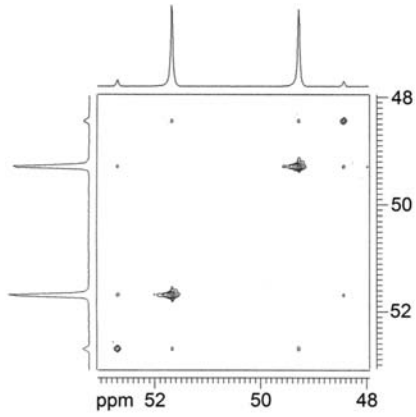

Figure 3. Expansion of the 100.6 MHz 2D $^{13}C\{^1H\}$ EXSY NMR spectrum of **1** in CD_2Cl_2 at 219.8 K. Exchange peaks between the Me_2N groups are shown. The mixing time was 100 ms.

It is clear that the Me_2N groups are chemically inequivalent at this temperature because they appear as two equal-area resonances around δ 2.79 and 2.73. It is also clear that these two major resonances are flanked by two minor, equal-area resonances at δ 2.82 and 2.68. The major to minor isomer resonances are in an area ratio of about 7:1. The CH_2N resonances that comprise an AA′XX′ spin system in slow exchange appear as two equal-area features at around δ 3.37 and 2.23. Within each CH_2N multiplet, there are features for the major and minor isomers that cannot be separated in the 1D spectrum because of the complexity of the spin system, resulting in a relatively broad splitting pattern and a small population of the minor isomer. Integration of the ^{1}H NMR spectrum supports the assertion that CH_2N resonances of both major and minor isomers are overlapped. The initial interpretation of the 1D ^{1}H NMR spectrum is that (a) ring inversion of the five-membered Th-tmed ring is slow at 220 K and (b) two isomers are present at this temperature. This interpretation is supported by the less complex $^{13}C\{^1H\}$ NMR spectrum, shown in Figure 2. The ^{13}C NMR spectrum consists of two inequivalent Me_2N resonances at δ 51.7 and 49.3 along with a single resonance due to the backbone CH_2N group at δ 58.0 due to the major isomer. These major isomer resonances are flanked by resonances due to the minor isomer at δ 52.7 and 48.4 (Me_2N) and δ 57.8 (CH_2N).

The most important NMR spectrum is shown in Figure 3. The EXSY spectrum shows the exchange network in which each Me_2N resonance of the major isomer can exchange into either of the chemically inequivalent Me_2N sites in the minor isomer and vice versa. The mixing time was kept deliberately short to avoid significant intensity of cross peaks that are due to the buildup of two-step processes. All of the off-diagonal exchange peaks in Figure 3 are between different isomers. There are no cross peaks that indicate the exchange of methyl groups within the same isomer, either major or minor. Thus, the Me_2N groups on the major isomer do not directly exchange with themselves; they indirectly exchange pairwise through the minor isomer. Two steps are required to change the location of a methyl group from one chemically distinct environment in the major isomer to another chemically distinct environment in the major isomer. This involves major to minor and then minor back to major isomer exchange steps. Further, the exchange process does not proceed via a geometry in which all of the Me_2N groups are equivalent because such a process would show off-diagonal peaks between all four methyl resonances. The physical process is intramolecular because no exchange is detected between free and bound tmed on the NMR time scale when additional tmed is present. No free tmed is observed in the spectra of **1**.

In addition to the exchange of methyl groups, the EXSY spectrum indicates an exchange of the backbone CH_2N C atoms in the major isomer with the CH_2N C atoms in the minor isomer at a corresponding rate (spectra in the Supporting Information).

The exchange rate at 220 K from the major isomer methyl sites into the minor isomer sites is 0.41 ± 0.09 s^{-1} (average of four values ranging from 0.36 to 0.48 s^{-1}). The rate of the reverse process, minor-to-major isomer conversion is 4.0 ± 1.1

dx.doi.org/10.1021/ic300586f | Inorg. Chem. 2012, 51, 10141−10147

s^{-1} (again an average of four values), predictably faster based upon the equilibrium ratio of ≈8:1 observed in the $^{13}C\{^1H\}$ NMR spectrum. The activation barrier for the major-to-minor interconversion process is therefore $\Delta G^{\ddagger}_{220\ K} = 13.1 \pm 0.1$ kcal mol^{-1}.

We turn now to the structures of the two isomers. Figure 4 shows the four possible configurations of the two tmed ligands in **1**.

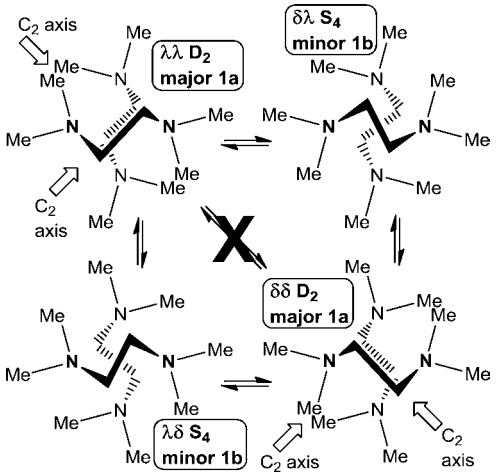

Figure 4. Simplified views showing only the tmed ligands of the four possible bischelate conformations of **1**, $\delta\delta$, $\delta\lambda$, $\lambda\delta$, and $\lambda\lambda$. Permitted exchange processes are also indicated. Species are drawn such that the C_2 axis that runs through the midpoints of both tmed C−C bonds (and the Th atom) is perpendicular to the page in all four structures.

Each of the five-membered chelate rings introduces an element of chirality into the molecule, commonly referred to as δ and λ configurations (Figure 5). In the $\delta\delta$ and $\lambda\lambda$ isomers, the projections of the CH_2-CH_2 bonds of the two tmed ligands are close to parallel. By contrast, in the $\delta\lambda$ and $\lambda\delta$ isomers, the projections of the CH_2-CH_2 bonds of the two tmed ligands are crossed. These two orientations result in complexes with slightly different Gibb's free energies. The X-ray structure of the analogous uranium complex, $UCl_4(tmed)_2$, indicates that the preferred geometry in the solid state has a parallel arrangement of the CH_2-CH_2 bonds, i.e., $\delta\delta$ or $\lambda\lambda$. The major isomer of **1** in solution is therefore proposed to have the same $\delta\delta$ or $\lambda\lambda$ geometry (**1a**), as shown in Figure 4. In **1a**, each of the tmed rings has the same configuration, either $\delta\delta$ or $\lambda\lambda$, with the two options being enantiomers of each other, and the point group is D_2. In the alternative conformations, with the near-perpendicular projection of tmed CH_2-CH_2 bonds, the two tmed rings have opposite configurations, $\delta\lambda$ or $\lambda\delta$ (**1b**, meso compounds), and the point group is S_4; **1a** is assigned as the major isomer, and **1b** is assigned as the minor isomer. While the DFT calculations (see below) on the whole support these assignments of major and minor isomers, the two isomers are close in energy and the possibility that the assignments should actually be reversed cannot be discounted. The assignment of the stereochemistry of the isomers does not affect the interpretation of the exchange mechanism. If a simultaneous switching of ligands were present, directly converting $\delta\delta$ with $\lambda\lambda$ and/or $\delta\lambda$ with $\lambda\delta$, then direct exchange peaks between the axial and equatorial methyl groups within the major or minor isomer would be observed. This is not the case.

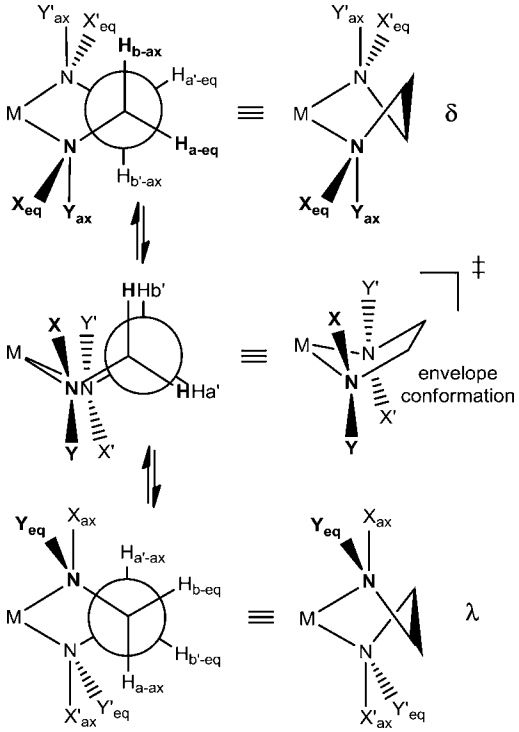

Figure 5. δ and λ conformations of a single chelated tmed ligand highlighting axial and equatorial substituent positions and their possible interchange via an envelope conformation (κ^2 mechanism).

We assert that the physical process giving rise to the EXSY spectrum in Figure 3 involves ring inversion ($\delta \leftrightarrow \lambda$) of one of the five-membered chelate rings. This can proceed either without breaking of a Th−N bond, as shown in Figure 5, or through a process that breaks one of the Th−N bonds. The NMR data cannot distinguish between these two pathways. The inversion of one (but not both) of the tmed rings is consistent with the exchange pattern observed in the EXSY spectrum; for example, an axial methyl group in the major isomer can exchange into either an axial or equatorial methyl site on the minor isomer. The inversion of just one ring always interconverts the major and minor isomers. The inversion process results in the exchange of axial and equatorial sites within the ligand that inverts at the same time as the isomer is switched. The other ligand does not invert and, therefore, while the switch of isomers still occurs for this ligand during an exchange event, the methyl groups in the axial and equatorial sites remain in these sites. Hence, there is equal probability that, when isomerization occurs, a given methyl group will stay in the same type of site, axial or equatorial, or switch sites. Through this mechanism, the exchange of an axial site in the major isomer with an equatorial site in the major isomer requires two successive inversions of both of the tmed chelates, resulting in an overall change of the major isomer enantiomer in the process [$\delta\delta$ (major) → $\delta\lambda$ (minor) → $\lambda\lambda$ (major)]. This ring inversion involves a change in symmetry along the reaction coordinate as $D_2 \leftrightarrow S_4 \leftrightarrow D_2$. A corollary of this postulate is that, if the enantiomers were resolved, ring inversion would result in racemization. A simultaneous switch of both ligands [e.g., $\delta\delta$ (major) → $\lambda\lambda$ (major)] is not consistent with the EXSY data.

If dissociation of tmed to afford free tmed in undetectably low quantities were involved in the exchange mechanism, i.e., in an intermolecular process, a direct exchange between all four

dx.doi.org/10.1021/ic300586f | Inorg. Chem. 2012, 51, 10141−10147

methyl resonances would be expected. This is because the free tmed ligand would undergo scrambling of δ and λ configurations upon recoordination. The free ligand is required to rapidly associate with a different thorium center because only bound tmed ligands are detected in the EXSY spectrum. This different thorium center would have a second tmed ligand attached with a statistical mixture of δ and λ ligands. By this mechanism, a direct exchange of $\delta\delta$ and $\lambda\lambda$ isomers is possible, contrary to the experimental observations. This provides further confirmation that the exchange process is intramolecular. Similarly, a mechanism involving binuclear complexes with bridging tmed ligands, i.e., Th−N(Me_2)-CH_2CH_2(Me_2)N−Th is likewise extremely unlikely because this would also result in the transfer of tmed ligands from one thorium center to another. Rotation around single bonds in the bridging tmed ligands is likely to allow facile interconversion of δ and λ for the bridging ligand upon transfer and then rechelation. In turn, the bridging ligand that undergoes transfer may also be transferred to a thorium center in which the other tmed ligand has a configuration opposite to that of the second tmed ligand that was present on the thorium center to which the tmed ligand undergoing transfer was initially bound. Again, this would give $\delta\delta$-to-$\lambda\lambda$ direct interconversion on occasion, which is inconsistent with the observed pattern in the EXSY spectra.

Computational Investigation of the Exchange Mechanism. The intimate mechanism by which the exchange occurs was investigated using DFT. As was already noted, NMR spectroscopy can determine which sites within different isomers are exchanging but not how the process is occurring. In **1**, the data indicate that one, and only one, of the tmed rings is inverting. We considered two likely possibilities for inverting the tmed ligand in this case: (i) the κ^2 mechanism, in which both N-donor atoms remain coordinated throughout the inversion process; (ii) the κ^1 mechanism, in which one of the Th−N bonds is broken during the exchange process and subsequent rotations around single bonds in the now monodentate tmed ligand and recoordination of the N-donor atom lead to inversion of the tmed ligand.

The possible inversion pathways were studied initially using the B3PW91 functional in a vacuum, which has been found to give satisfactory geometries for actinide complexes.[21,22] The appropriateness of the functional for predicting molecular geometries in **1** was tested by calculating an optimized geometry of the analogous uranium compound, $UCl_4(tmed)_2$ (triplet, unrestricted open-shell calculation). The average U−N bond distances were 0.086 Å longer in the calculated structure (2.872 Å) compared to the X-ray structure (2.786 Å), but the U−Cl distances were only 0.008 Å longer, on average, in the calculated structure (2.617 Å) compared to the X-ray structure (2.609 Å). The method was thus deemed satisfactory for this class of complexes.

In the case of the major isomer of **1a** (singlet, restricted closed-shell calculation), the calculated metal-donor atom distances are predictably slightly longer than found in the uranium complex, with Th−N distances of 2.893 Å and Th−Cl distances of 2.683 Å, because the radii of Th^{IV} and U^{IV} in eight-coordination differ by 0.05 Å.[23] A natural bond order (NBO) analysis of the Th−N bond shows that it is highly polarized, with 93.5% of the NBO on the N hybrid orbitals and 6.5% of the NBO on the Th hybrids, as is the Th−Cl bond, 85.7% on Cl and 14.3% on Th. In addition, each of the lone pairs on Cl contribute to the Th−Cl bond (93% on Cl and 6.9% on Th). The NBO charges on Th (+0.57), N (−0.62), and Cl (−0.35) also support the intuitive view that the bonds are polarized. The Th−N distances are noticeably long compared to the sum of the ionic radii of eight-coordinate Th^{4+} and N^{3-} (2.51 Å),[23] suggesting that the Th−N bond may be relatively weak.

The minor isomer has almost identical metal−ligand bond lengths (Th−N 2.900 Å; Th−Cl 2.681 Å). The geometries of the major and minor isomers of **1**, when optimized without any symmetry constraints, converge to structures that are negligibly different from D_2 and S_4 symmetries in the case of **1a** and **1b**, respectively. The energies of the two species **1a** and **1b** are similar. The minor isomer **1b** is calculated to be 0.6 kcal mol^{-1} higher in energy than **1a** if C_1 symmetry is assumed (ΔG at 220 K) and 0.1 kcal mol^{-1} if D_2 and S_4 symmetries are imposed. This agrees with the observed 8:1 major-to-minor isomer equilibrium ratio (experimental $\Delta G_{220\ K}$ = 0.9 kcal mol^{-1}). As noted above, because **1a** and **1b** are close in energy, it is possible that the assignment of major and minor isomers could be reversed.

The first plausible mechanism for ligand inversion is shown in Figures 5 and 6.

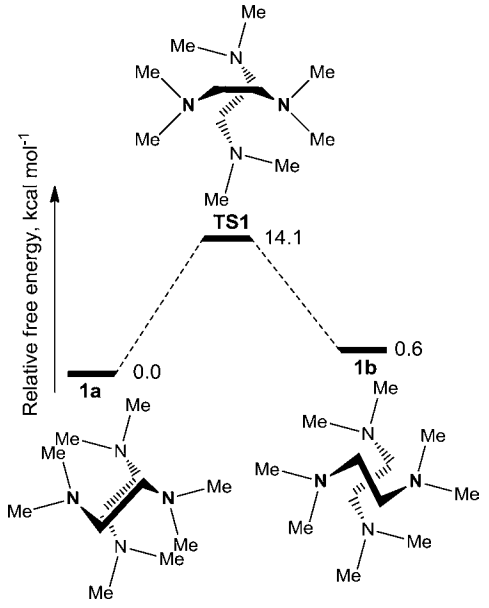

Figure 6. Energy profile for the inversion process in **1** connecting **1a** and **1b** via the κ^2 mechanism.

The inversion process proceeds via an envelope transition structure (Figure 5),[11] TS1, in which the N−C−C−N dihedral angle is close to zero (0.6° calculated). The Th atom is 33° out of the plane formed by the inverting tmed ligand in TS1. The Th−N distances of the inverting structure are 2.890 and 2.928 Å, almost unchanged from the Th−N distances in the major and minor isomers. The inversion process via this route may be viewed as requiring a change in the dihedral angles of each of the three bonds in the N−C−C−N backbone of the tmed ligand. The energy of TS1 is 14.1 kcal mol^{-1} ($\Delta G_{220\ K}$) higher in energy than the major isomer **1a**, similar to the observed activation barrier $\Delta G^{\ddagger}_{220\ K}$ = 13.1 kcal mol^{-1} for conversion of **1a** to **1b**.

The second plausible mechanism, the κ^1 mechanism, for the ligand inversion is shown in Figure 7. From left to right, starting from the major isomer **1a**, the mechanism proceeds initially via dissociation of one of the tmed N−Th bonds. The activation

dx.doi.org/10.1021/ic300586f | Inorg. Chem. 2012, 51, 10141−10147

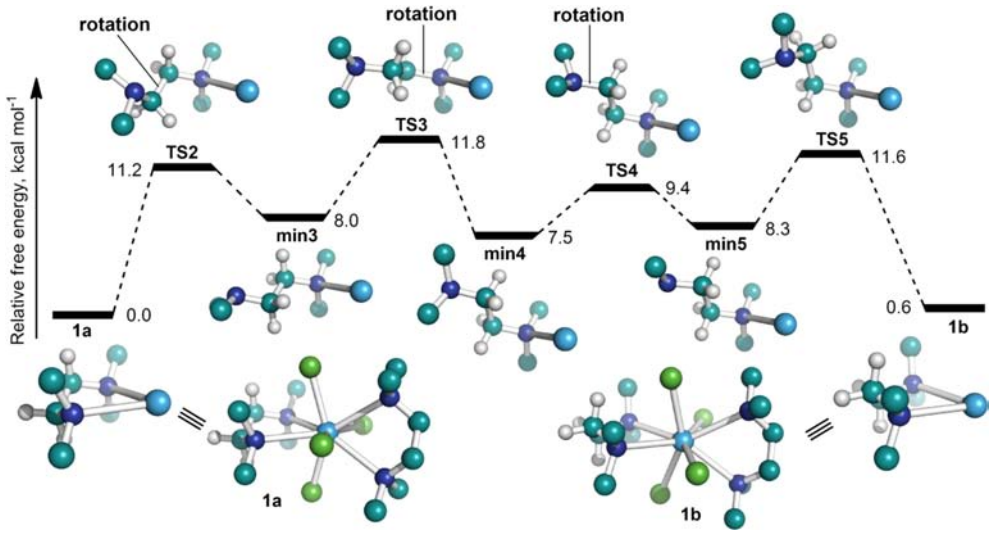

Figure 7. Energy profile for the inversion process in **1** connecting **1a** and **1b** via the κ^1 mechanism. Only the inverting tmed ligand is shown; the other remains unchanged. B3PW91 free-energy values in a vacuum are shown (see also Table 2).

barrier for breaking a Th−N bond is relatively low in this complex, with $\Delta G^{\ddagger}_{220\ K}$ = 11.2 kcal mol^{-1} (B3PW91, vacuum) for TS2. This transition structure TS2 (Th−N = 4.32 Å) coincides with the substituents on the C−C bond of the tmed ligand being placed in an eclipsed conformation. Rotation around the C−C bond of tmed occurs as matter of course as the Th−N bond is lengthened starting from structure **1a**. Hence, the barrier at transition structure TS2 may be viewed as being due to a rotation of substituents around a single bond rather than simply a barrier to the breaking of the Th−N bond. After breaking the Th−N bond, the structure finds a local energy minimum, min3 (Th−N = 5.07 Å), with a κ^1-tmed ligand and ΔG = 8.0 kcal mol^{-1} relative to **1a**.

Starting from min3, in order to interconvert the δ and λ configurations of **1**, a dihedral rotation of ca. 120° about both of the CH_2−N bonds is required prior to recoordination of the uncomplexed nitrogen. Rotation around the complexed N−CH_2 bond proceeds via an eclipsed transition structure, TS3, with $\Delta G^{\ddagger}$ = 11.8 kcal mol^{-1} relative to **1a** through to a local minimum, min4, with a relative energy of 7.5 kcal mol^{-1}. TS3 is found to be the highest barrier on the potential energy surface of Figure 7. Again the TS3 barrier of 11.8 kcal mol^{-1} is similar to the observed activation barrier for this process ($\Delta G^{\ddagger}$ = 13.1 kcal mol^{-1}), and therefore it is possible that this is the mechanism operating. Subsequent rotation around the uncomplexed N−CH_2 bond proceeds through a transition structure, TS4, with $\Delta G^{\ddagger}$ = 9.4 kcal mol^{-1} (a slightly lower barrier compared to TS3), to a new local minimum, min5. This local minimum, min5, is the same structure that is found when a Th−N bond in the minor isomer **1b** is broken, going through transition structure TS5 ($\Delta G^{\ddagger}$ = 11.6 kcal mol^{-1}; Th−N = 4.33 Å). Thus, the microscopic reverse proceeding from min5 to form the Th−N bond completes the tmed ring-inversion process via the κ^1 mechanism. Changing the order of rotation of the two CH_2−N bonds makes little difference to the highest activation barrier (0.6 kcal mol^{-1} higher in energy compared to TS3).

We note that inversion at the N atom that is not coordinated starting from a point such as min3 in the possible mechanism was not considered computationally for two reasons. First, an inversion at the N atom and subsequent recoordination could swap equatorial and axial type methyl groups without leading to a different isomer of **1** and so is inconsistent with the observed EXSY data. Second, the barrier to inversion at the N atom is known to be significantly larger than the barrier to rotation around single bonds in the monodentate tmed ligand, which can ultimately lead to inversion of the chelate ring. For example, the experimental barrier to inversion in ethyldimethylamine is $\Delta G^{\ddagger}_{199\ K}$ = 8.6 kcal mol^{-1},[24] and this will lead to a significantly higher barrier than TS3.

The similarity of the activation barriers for the κ^1 and κ^2 mechanisms in this case leads to the conclusion that either mechanism is a realistic possibility in **1**. Further insight into which of the two mechanisms is likely to be operating was sought by examining the effect of applying different functional, dispersion corrections and the effect of solvent on the key components of the energy profile, specifically the energies of the highest transition states (TS1, TS3, and TS5) compared to major and minor isomers. The M06 functional was employed because it has been found to perform well in studies of actinide complexes.[25,26]

Table 2 summarizes the relative energies (ΔE) and relative free energies (ΔG) of selected species, with and without solvation using the B3PW91 and M06 functionals. The effect of including the dispersion corrections of Grimme and coworkers[27] is also included in the table.

The values in the table are calculated without symmetry constraints for **1a** and **1b**, assuming C_1 symmetry. Restricting the isomer to D_2 symmetry in the case of **1a** and S_4 symmetry in the case of **1b** increases the relative free energies of **1a** by ca. 0.6 kcal mol^{-1} and **1b** by 0.1−0.4 kcal mol^{-1} (see the Supporting Information), largely because the higher symmetry leads to less rotational entropy. So, if the point-group symmetry is retained in solution, the calculated activation barriers quoted would be reduced by ca. 0.6 kcal mol^{-1}.

The most important values to compare in Table 2 are those for TS1, the highest barrier on the κ^2 mechanism, and TS3, the highest barrier on the κ^1 mechanism, because the relative magnitudes of these values will determine which inversion path is followed. The calculated barrier for the κ^2 mechanism via TS1 is relatively invariant with respect to the changing method, inclusion of solvent, or dispersion corrections, $\Delta G^{\ddagger}$ ranging

dx.doi.org/10.1021/ic300586f | Inorg. Chem. 2012, 51, 10141−10147

Table 2. Relative Energies of Key Structures Found in Potential Inversion Mechanisms of the tmed Ligand in 1

		species					
method	type[a]	**1a**	**1b**	TS1	TS3	min5	TS5
B3PW91	ΔE_{vac}	0.0	0.5	14.0	13.5	10.5	12.6
B3PW91	ΔG_{vac}	0.0	0.6	14.1	11.8	8.3	11.6
B3PW91	ΔE_{PCM}	0.0	0.6	13.6	11.8	7.8	6.7
B3PW91	ΔE_{D3}	0.0	0.7	14.8	20.4	17.7	18.7
B3PW91	ΔG_{all}	0.0	0.9	14.4	17.0	12.6	11.8
M06	ΔE_{vac}	0.0	0.5	14.1	19.7	16.8	17.4
M06	ΔG_{vac}	0.0	0.2	13.7	19.0	15.1	16.5
M06	ΔE_{PCM}	0.0	0.7	13.7	18.2	14.9	12.8
M06	ΔE_{D3}	0.0	0.6	14.1	19.8	17.2	17.7
M06	ΔG_{all}	0.0	0.5	13.4	17.6	13.6	12.2

[a]Types: ΔE_{vac} = energy in a vacuum; ΔG_{vac} = free energy in a vacuum at 220 K; ΔE_{PCM} = energy in PCM dichloromethane; ΔE_{D3} = energy in a vacuum with D3 corrections, i.e., B3PW91-D3 and M06-D3; ΔG_{all} = free energies at 220 K using electronic energies in PCM solvent with D3 and vacuum thermochemical corrections. All ΔE values include zero-point vibrational energy calculated in a vacuum.

from 13.4 to 14.1 kcal mol^{-1}, which agrees well with the observed barrier.

In contrast, the calculated barrier for the κ^1 mechanism via TS3 is highly dependent on functional, dispersion corrections and the inclusion of solvent, with $\Delta G^{\ddagger}$ values ranging from 10.1 to 19.1 kcal mol^{-1}. The newer M06 functional suggests that barriers are larger by about 6–7 kcal mol^{-1} compared to those of the unmodified B3PW91 functional. The B3PW91-D3 energy of TS3 is increased by 6.9 kcal mol^{-1} compared to that of unmodified B3PW91. Thus, inclusion of dispersion through D3 corrections makes the difference between functionals much less, with calculated energies of TS3 for the B3PW91-D3 and M06(-D3) methods differing by less than 1 kcal mol^{-1}. Because the M06 functional is designed to implicitly account for dispersion interactions, the D3 corrections are predictably small. Inclusion of dispersion interactions has been shown to improve the prediction of metal–ligand bond strengths in the case transition metal–phosphorus bonds at least.[28,29] In cases such as the thorium complex **1** discussed here, where the metal–nitrogen bond is weak and the central atom is heavy, the dispersion energy may constitute a significant fraction of the metal–nitrogen bond dissociation energy. Inclusion of solvent lowers the TS3 barrier in the κ^1 mechanism by 1.5–1.7 kcal mol^{-1}. The inclusion of solvent stabilizes all species with a broken (or breaking) Th–N bond. This is unsurprising given the possibility that dichloromethane can act as a weak donor ligand.

It is clear that the transition structure for breaking of the Th–N bond in **1b**, TS4, calculated in a vacuum is not a transition structure when the solvent is included (single-point calculations) because the completely dissociated structure min5 (broken Th–N distance = 5.09 Å, B3PW91) is slightly higher in energy than TS4 ("breaking" Th–N distance = 4.39 Å) when solvent effects are included. The highest point on the potential energy surface for the κ^1 mechanism, TS3, contains a fully dissociated N atom and the barrier corresponds to rotation of a dihedral angle through an eclipsed transition structure. The geometry of this transition structure is likely to be relatively insensitive to the inclusion of PCM solvent.

In short, the B3PW91 functional without dispersion correction predicts the κ^1 mechanism to be preferred, whereas M06(-D3) and B3PW91-D3 functionals predict that the κ^2 mechanism is preferred. In practice, the closeness of the barriers prevents a clear distinction between the two mechanisms. On balance, the κ^2 mechanism appears slightly more likely because methods that account for dispersion favor this pathway, but because the difference in energy is only 3.6–4.2 kcal mol^{-1} (ΔG_{all}), both pathways are possible.

CONCLUSIONS

The 2D NMR spectra of **1** give mechanistic details that are not available in the 1D spectra. The 1D ^{1}H and ^{13}C{^{1}H} spectra show that two isomers are present in a ratio of ≈8:1 at low temperatures and that the methyl groups in Me_2N are chemically inequivalent at 219.8 K in both isomers. Thus, ring inversion in the eight-coordinate complex is slow at this temperature. The ^{13}C{^{1}H} EXSY NMR spectrum shows that the inequivalent axial and equatorial methyl groups in the major isomer exchange only with the inequivalent methyl groups in the minor isomer. This result leads to the postulate that interconversion of enantiomers of the major isomer proceeds via a two-step pathway in which the first step involves a ring inversion of one tmed ligand, leading to the minor isomer. A subsequent ring inversion of the second tmed ligand leads to the major isomer once more, this time as the opposite enantiomer. The postulate of axial and equatorial methyl group exchange also exchanges the orientation of the ethylene backbones in the two tmed ligands that are aligned essentially parallel in the major isomer and perpendicular in the minor isomer. The perpendicular alignment of the two ethylene groups has a slightly higher Gibb's free energy than the parallel alignment, and this difference accounts for the observation of the two isomers at low temperature in the ≈8:1 ratio and allows their exchange to be detected in the EXSY spectrum. The rate of conversion of the major-to-minor isomer is 0.41 s^{-1} at 219.8 K ($\Delta G^{\ddagger}$ = 13.1 kcal mol^{-1}).

Computational investigations indicate that the exchange process may occur either without dissociation of a N-donor atom, a κ^2 mechanism through an envelope transition structure, or with dissociation of one N-donor atom and subsequent rotation around single bonds, a κ^1 mechanism. In general terms for other complexes, a larger bond dissociation energy of the chelate donor will make the κ^1 mechanism less likely. In complexes where the metal–donor ligand bond is weak, as in the present example, it is difficult to design experiments that distinguish between the κ^1 and κ^2 mechanisms, unless the complexes are without symmetry.[30]

EXPERIMENTAL SECTION

$ThCl_4(tmed)_2$ (**1**) was synthesized as described previously.[15a]

NMR Spectroscopy. Experiments were conducted on a 400 MHz instrument, operating at 100.6 MHz for ^{13}C NMR. The temperature was measured using a sample of methanol.[31] The 2D ^{13}C EXSY NMR experiment employed a standard pure-phase (TPPI) NOESY pulse sequence with ^{1}H decoupling throughout. The spectral width was 1055.1 Hz in both dimensions, with 393 × 1K points, 32 scans each, collected in t_1 and t_2, respectively. The acquisition time was 0.48 s, the recycle delay was 0.8 s, and 90° pulses were 5.7 μs in duration. The mixing time was 100 ms. Volume integration of the spectrum and the program *EXSYCalc*[32] were used to extract rate constants.[33,34]

Computational Methods. DFT calculations were performed using the *Gaussian09* software package,[35] revision A for calculations employing the B3PW91[36,37] and B3LYP[36,38] functionals and revision B for M06[39] calculations. Geometry optimizations and frequency/thermochemical calculations were conducted in a vacuum using the

B3PW91 and M06 functionals with basis set 1, BS1. The BS1 basis consisted of the Stuttgart/Dresden effective core potential for Cl atoms[40] and an associated basis set (SDDall) with an additional polarization function (*d* exponent = 0.643)[41] and the 6-31G(d,p) basis set[42] for all other elements except thorium. The Th atoms employed the Stuttgart/Dresden effective core potential MWB60[43] and the ECP60MWB_SEG segmented basis set.[44]

Single-point-energy calculations employed the larger basis set, BS2, consisting of the same basis set for the Th atoms and 6-311+G(2d,p) for all of the other atoms. Energy values quoted in the paper are method/BS2//method/BS1 and include correction for the zero-point vibrational energy (calculated using BS1 in a vacuum). Free-energy values, *G*, were calculated at 220 K and 1 atm. DFT calculations for thorium complexes were performed using restricted closed-shell wave functions. All minimum-energy structures for the metal complexes were initially calculated without any symmetry constraints and were confirmed to be minima by calculating their normal vibrations within the harmonic approximation and observing that there were no imaginary frequencies. Transition structures were confirmed to have one imaginary frequency. Scaling factors used for the zero-point vibrational energy values were 0.9799 for B3PW91[45] and 0.98 for M06.[46] NBO calculations were performed using NBO version 3.1, as implemented in the G09 program with HF/BS2 employed. Graphics were generated using the *Pymol* software package.[47] Where calculations in solvent are indicated, the calculations were single point, employing the vacuum geometries and the default solvent method implemented in *Gaussian09* (IEFPCM) with dichloromethane as the solvent. Single-point DFT-D3 dispersion corrections were calculated using the *DFT-D3* program, version 2.0 revision 1, using geometries from an uncorrected functional.[27]

■ ASSOCIATED CONTENT

Ⓢ Supporting Information

Complete EXSY spectrum and other expansions, tables summarizing the DFT results, and calculated coordinates of minima and transition structures from Figures 6 and 7 and Table 2. This material is available free of charge via the Internet at http://pubs.acs.org.

■ AUTHOR INFORMATION

Corresponding Author

*E-mail: g.ball@unsw.edu.au (G.E.B.), raandersen@lbl.gov (R.A.A.).

Notes

The authors declare no competing financial interest.

■ ACKNOWLEDGMENTS

This work was supported by the Director, Office of Science, Office of Basic Energy Sciences (OBES), of the U.S. Department of Energy (DOE) under Contract DE-AC02-05CH11231. Computational work was supported by an award under the Merit Allocation Scheme through INTERSECT on the Australian NCI National Facility. The authors thank Drs. Mark Petrie, Marc Weydert, and Wayne Lukens for their help with sample preparation.

■ REFERENCES

(1) Kepert, D. L. Inorganic Chemistry Concepts. *Inorganic Stereochemistry*; Springer-Verlag: Heidelberg, Germany, 1982; Vol. 6.
(2) Porari-Koshits, M. A.; Aslanov, L. A. *J. Struct. Chem.* **1972**, *13*, 244.
(3) Muetterties, E. L.; Guggenberger, L. J. *J. Am. Chem. Soc.* **1974**, *96*, 1748.
(4) Holm, R. H. *Dyn. Nucl. Magn. Reson. Spectrosc.* **1975**, 317.
(5) Holm, R. H.; Hawkins, C. J. *NMR Paramagn. Mol.* **1973**, 243.
(6) Grdenic, D.; Matkovic, B. *Acta Crystallogr.* **1959**, *12*, 817.
(7) Titze, H. *Acta Chem. Scand.* **1970**, *24*, 405.
(8) Steffen, W. L.; Fay, R. C. *Inorg. Chem.* **1978**, *17*, 779.
(9) Fay, R. C.; Howie, J. K. *J. Am. Chem. Soc.* **1977**, *99*, 8110.
(10) Hawkins, C. J.; Palmer, J. A. *Coord. Chem. Rev.* **1982**, *44*, 1.
(11) Hawkins, C. J.; Peachey, R. M.; Szoredi, C. L. *Aust. J. Chem.* **1978**, *31*, 973.
(12) Caulton, K. G. *Inorg. Nucl. Chem. Lett.* **1973**, *9*, 533.
(13) Evans, D. F.; De Villardi, G. C. *J. Chem. Soc., Chem. Commun.* **1976**, 7.
(14) Evans, D. F.; De Villardi, G. C. *J. Chem. Soc., Dalton Trans.* **1978**, 315.
(15) (a) Edwards, P. G.; Weydert, M.; Petrie, M. A.; Andersen, R. A. *J. Alloys Compd.* **1994**, *213/214*, 11. (b) Ren, W.; Zi, G.; Fang, D.-C.; Walter, M. *Chem.—Eur. J.* **2011**, *17*, 12669. (c) Ren, W.; Zi, G.; Fang, D.-C.; Walter, M. *J. Am. Chem. Soc.* **2011**, *133*, 13183.
(16) Hargraves, R.; Moir, R. *Am. Sci.* **2010**, *98*, 304.
(17) Rodriguez, P.; Sundaram, C. V. *J. Nucl. Mater.* **1981**, *100*, 227.
(18) Jacoby, M. *Chem. Eng. News* **2009**, *87*, 44.
(19) Zalkin, A.; Edwards, P. G.; Zhang, D.; Andersen, R. A. *Acta Crystallogr., Sect. C: Cryst. Struct. Commun.* **1986**, *C42*, 1480.
(20) Cotton, F. A.; Wilkinson, G.; Murillo, C. A.; Bochmann, M. *Advanced inorganic chemistry*, 6th ed.; Wiley: New York, 1999; p 16.
(21) Maron, L.; Eisenstein, O.; Andersen, R. A. *Organometallics* **2009**, *28*, 3629.
(22) Barros, N.; Maynau, D.; Maron, L.; Eisenstein, O.; Zi, G.; Andersen, R. A. *Organometallics* **2007**, *26*, 5059.
(23) Shannon, R. D. *Acta Crystallogr., Sect. A* **1976**, *A32*, 751.
(24) Casarini, D.; Davalli, S.; Lunazzi, L.; Macciantelli, D. *J. Org. Chem.* **1989**, *54*, 4616.
(25) Averkiev, B. B.; Mantina, M.; Valero, R.; Infante, I.; Kovacs, A.; Truhlar, D. G.; Gagliardi, L. *Theor. Chem. Acc.* **2011**, *129*, 657.
(26) Austin, J. P.; Burton, N. A.; Hillier, I. H.; Sundararajan, M.; Vincent, M. A. *Phys. Chem. Chem. Phys.* **2009**, *11*, 1143.
(27) Grimme, S.; Antony, J.; Ehrlich, S.; Krieg, H. J. *Chem. Phys.* **2010**, *132*, 154104/1.
(28) Fey, N.; Ridgway, B. M.; Jover, J.; McMullin, C. L.; Harvey, J. N. *Dalton Trans.* **2011**, *40*, 11184.
(29) Minenkov, Y.; Occhipinti, G.; Jensen, V. R. *J. Phys. Chem. A* **2009**, *113*, 11833.
(30) Gogoll, A.; Oernebro, J.; Grennberg, H.; Bäckvall, J.-E. *J. Am. Chem. Soc.* **1994**, *116*, 3631.
(31) Van Geet, A. L. *Anal. Chem.* **1970**, *42*, 679.
(32) Cobas, J. C.; Martin-Pastor, M. *EXSYCalc*, 1.0 ed.; Mestrelab Research: Santiago de Compostela, Spain. Can be downloaded from http://mestrelab.com/software/exsycalc/.
(33) Perrin, C. L.; Dwyer, T. J. *Chem. Rev.* **1990**, *90*, 935.
(34) Zolnai, Z.; Juranic, N.; Vikic-Topic, D.; Macura, S. *J. Chem. Inf. Comput. Sci.* **2000**, *40*, 611.
(35) Frisch, M. J. et al. Gaussian, Inc.: Wallingford, CT, 2009. The full reference is given in the Supporting Information.
(36) Becke, A. D. *J. Chem. Phys.* **1993**, *98*, 5648.
(37) Perdew, J. P.; Wang, Y. *Phys. Rev. B* **1992**, *45*, 13244.
(38) Stephens, P. J.; Devlin, F. J.; Chabalowski, C. F.; Frisch, M. J. *J. Phys. Chem.* **1994**, *98*, 11623.
(39) Zhao, Y.; Truhlar, D. G. *Theor. Chem. Acc.* **2008**, *120*, 215.
(40) Bergner, A.; Dolg, M.; Kuechle, W.; Stoll, H.; Preuss, H. *Mol. Phys.* **1993**, *80*, 1431.
(41) Maron, L.; Teichteil, C. *Chem. Phys.* **1998**, *237*, 105.
(42) Hariharan, P. C.; Pople, J. A. *Theor. Chim. Acta* **1973**, *28*, 213.
(43) Kuechle, W.; Dolg, M.; Stoll, H.; Preuss, H. *J. Chem. Phys.* **1994**, *100*, 7535.
(44) Cao, X.; Dolg, M.; Stoll, H. *J. Chem. Phys.* **2003**, *118*, 487.
(45) Merrick, J. P.; Moran, D.; Radom, L. *J. Phys. Chem. A* **2007**, *111*, 11683.
(46) Alecu, I. M.; Zheng, J.; Zhao, Y.; Truhlar, D. G. *J. Chem. Theory Comput.* **2010**, *6*, 2872.
(47) Delano, W. L. *The PyMOL Molecular Graphics System*; Delano Scientific, LLC: Palo Alto, CA, 2006.